

ARTICLE



<https://doi.org/10.1038/s41467-020-15007-3>

OPEN

Liquid-liquid phase separation and extracellular multivalent interactions in the tale of galectin-3

Yi-Ping Chiu^{1,4}, Yung-Chen Sun^{1,4}, De-Chen Qiu¹, Yu-Hao Lin¹, Yin-Quan Chen², Jean-Cheng Kuo^{1,2} & Jie-rong Huang^{1,3}✉

Liquid-liquid phase separation (LLPS) explains many intracellular activities, but its role in extracellular functions has not been studied to the same extent. Here we report how LLPS mediates the extracellular function of galectin-3, the only monomeric member of the galectin family. The mechanism through which galectin-3 agglutinates (acting as a “bridge” to aggregate glycosylated molecules) is largely unknown. Our data show that its N-terminal domain (NTD) undergoes LLPS driven by interactions between its aromatic residues (two tryptophans and 10 tyrosines). Our lipopolysaccharide (LPS) micelle model shows that the NTDs form multiple weak interactions to other galectin-3 and then aggregate LPS micelles. Aggregation is reversed when interactions between the LPS and the carbohydrate recognition domains are blocked by lactose. The proposed mechanism explains many of galectin-3’s functions and suggests that the aromatic residues in the NTD are interesting drug design targets.

¹ Institute of Biochemistry and Molecular Biology, National Yang-Ming University, No. 155 Section 2 Li-nong Street, Taipei 11221, Taiwan. ² Cancer Progression Research Center, National Yang-Ming University, No. 155 Section 2 Li-nong Street, Taipei 11221, Taiwan. ³ Institute of Biomedical Informatics, National Yang-Ming University, No. 155 Section 2 Li-nong Street, Taipei 11221, Taiwan. ⁴These authors contributed equally: Yi-Ping Chiu, Yung-Chen Sun.

✉email: jierongh@ym.edu.tw

How molecules “know” where and when to react in the presence of multiple simultaneous cellular reactions is an open question. Lipid-bound membranes act as compartments that separate reactions (e.g., the synthesis of ATP inside mitochondria; the degradation of proteins inside lysosomes)¹, allowing them to progress efficiently. Another mechanism through which biological activities are regulated in cells is the formation of biomolecular condensates (also known as membraneless organelles), such as stress granules, nucleoli, and Cajal bodies². Although these condensates have been observed for decades, their biophysical properties have only recently been investigated^{2–4}. The formation of biomolecular condensates is governed by multivalent proteins that undergo LLPS⁵. RNA binding proteins such as hnRNP A1, hnRNP A2, FUS, and TDP-43 are some of the most studied examples. The multivalency of these proteins is typically the result of repeated amino-acid motifs in intrinsically disordered regions⁶, responsible for reversible aggregation and the formation of stress or RNA granules^{7–10}. On the other hand, dysregulated condensate formation, because of point mutations^{9,10} or post-translational modifications^{11,12}, can lead to pathological fibrilization. LLPS is also involved in DNA transcription regulation, notably in the functions of the disordered C-terminal domain of RNA-polymerase II and associated proteins^{13,14}, the disordered activation domains of transcription factors^{15–17}, and heterochromatin proteins^{18,19}. Other cellular functions also known to be mediated by LLPS include cell cycle control^{20,21}, synaptic transmission^{22,23}, autophagic degradation²⁴, cancer suppression²⁵, nuclear pore passage^{26,27}, protein quality control²⁸, and signal transduction^{29,30}. The question remains however whether LLPS, or the underlying mechanisms, also mediate functions in the extracellular milieu.

Cell-cell adhesion and extracellular signal response are reminiscent of granule formation and signal transduction inside cells. Lectins, which selectively bind to carbohydrates, are involved in many important extracellular functions such as cell agglutination and immune response³¹. Most lectins are membrane proteins, partially anchored to the cell membrane with outward carbohydrate-recognition domains (CRDs) that facilitate connections with other molecules (glycoproteins or glycolipids) on the surface of cells or in the extracellular matrix³¹. Galectins, however, the most widely expressed lectin subfamily, are freely expressed in the extracellular milieu without membrane-anchoring or glycosylation³². In 14 out of the 15 galectins, multivalency is the result of tandem-repeat CRDs or dimer formation. In contrast, galectin-3 is monomeric in solution and has just one CRD, which is tethered to an intrinsically disordered NTD, making it the only chimeric protein in the family. One of galectin-3’s functions is to agglutinate organelles, such as neutrophils and laminin^{33,34}, or glycosylated molecules^{35,36}. This function, in which multivalent galectin-3 acts as a “bridge”, is lost when the NTD is removed^{33,34,37,38}. The mechanism through which galectin-3 becomes multivalent is a matter of debate^{37,39–46}. A pentamer model³⁹ with cross-linking through the NTD has been proposed and is the most widely used^{35,36} explanation; however, there are no structural data to support this model and a large body of evidence indicates that galectin-3 is monomeric^{42,47–49}. We have previously demonstrated that the intrinsically disordered NTD interacts fuzzily, intermolecularly and intramolecularly, with the region of the CRD not involved in carbohydrate recognition, and that the NTD also self-associates (Fig. 1a–e)⁵⁰. An accumulation of weak self-associations may promote the formation of higher-order oligomers⁵¹; however, how these weak interactions of galectin-3 contribute to stronger interactions such as cell adhesion and signal transduction is unclear.

In this study, we demonstrate that galectin-3 LLPS is driven by interactions between aromatic residues in the NTD. Using

lipopolysaccharide (LPS) micelles as a model template, we show that this mechanism is also involved in full-length galectin-3’s extracellular agglutination function. The CRD binds the saccharide moiety on the surface of the micelles, increasing the local protein concentration. The resulting accumulation of multivalent NTD interactions transiently connects the monomers to each other in a manner resembling LLPS.

Results

Galectin-3 undergoes LLPS. To investigate galectin-3’s ability to agglutinate, we used LPS micelle as an in vitro assay^{40,52}. As shown previously, the higher the protein or LPS concentrations are, the more turbid the samples are (Fig. 1h, i, Supplementary Table 1, Supplementary Table 2)^{40,52}. As also reported previously^{33,34,37–39,42,47}, galectin-3 does not agglutinate in the absence of the NTD (Fig. 1j). This therefore raises the question of how the NTD makes monomeric galectin-3 multivalent (Fig. 1k).

The NTD of galectin-3 is prion-like according to the PLAAC algorithm (Fig. 1f)⁵³, and has a high probability of forming intermolecular interactions through aromatic residues according to predicted π - π interactions (Fig. 1g)⁵⁴. These properties are common in LLPS proteins⁵⁵. In a previous study, we observed that the NTD of galectin-3 self-associates but the CRD alone does not⁵⁰. Indeed, a 1 mM NTD sample with 150 mM NaCl condenses at higher temperatures and dissolves at lower ones in a reversible manner (Fig. 2a and Supplementary Movie 1), showing lower critical solution temperature (LCST) behavior^{56,57}. The coexistence curve could be determined using a temperature ramp search (Fig. 2a). Reducing the protein concentration increased the temperature of the transition boundary, as expected for LCST behavior (Supplementary Fig. 1a). We observed many instances of the condensates fusing (Fig. 2b and Supplementary Movie 2) and fluorescence recovery after photobleaching (FRAP) data also show that they have liquid-like properties (Fig. 2c, Supplementary Fig. 2). Increasing the salt or protein concentration promoted demixing of the protein (Fig. 2d). In the phase-diagram (Fig. 2e), the heterogeneous conditions (indicated as solid blocks) were all confirmed by distinguishing LCST behavior from aggregation. At the highest protein concentration (>2 mM), the NTD sample was homogenous at 15 °C and was heterogeneous at 30 °C in the absence of NaCl (Supplementary Fig. 1b).

We also tested whether full-length galectin-3 undergoes LLPS. We could not exceed concentrations of 600 μ M (~16 mg ml⁻¹) protein without precipitation and the highest concentration investigated was therefore 500 μ M. This sample only demixed at 30 °C when the NaCl concentration was increased above 600 mM. The phase diagram obtained is shown in Fig. 2f. All samples returned to a homogeneous state at 15 °C. Full-length galectin-3 also shows LCST phase separation (Fig. 2g and Supplementary Movie 3) and has liquid-like properties as confirmed by fluorescence microscopy and FRAP experiments (Fig. 2h). We determined that condensation was not the result of salting-out because the CRD alone and a full-length construct without aromatic residues in the NTD remained in a single phase under the same conditions (see below). Furthermore, at a high enough concentration, the NTD phase separated in the absence of NaCl (Supplementary Fig. 1b). The fact that the NTD and full-length galectin-3 undergo LLPS suggests that the multivalent connections involving the NTD also promote agglutination. We therefore investigated the mechanism driving these multivalent interactions.

Aromatic residues contribute to LLPS of the NTD of galectin-3. Sequence alignment indicates that the CRDs of galectin-3 are highly conserved among vertebrates (Fig. 3a, orange blocks), and

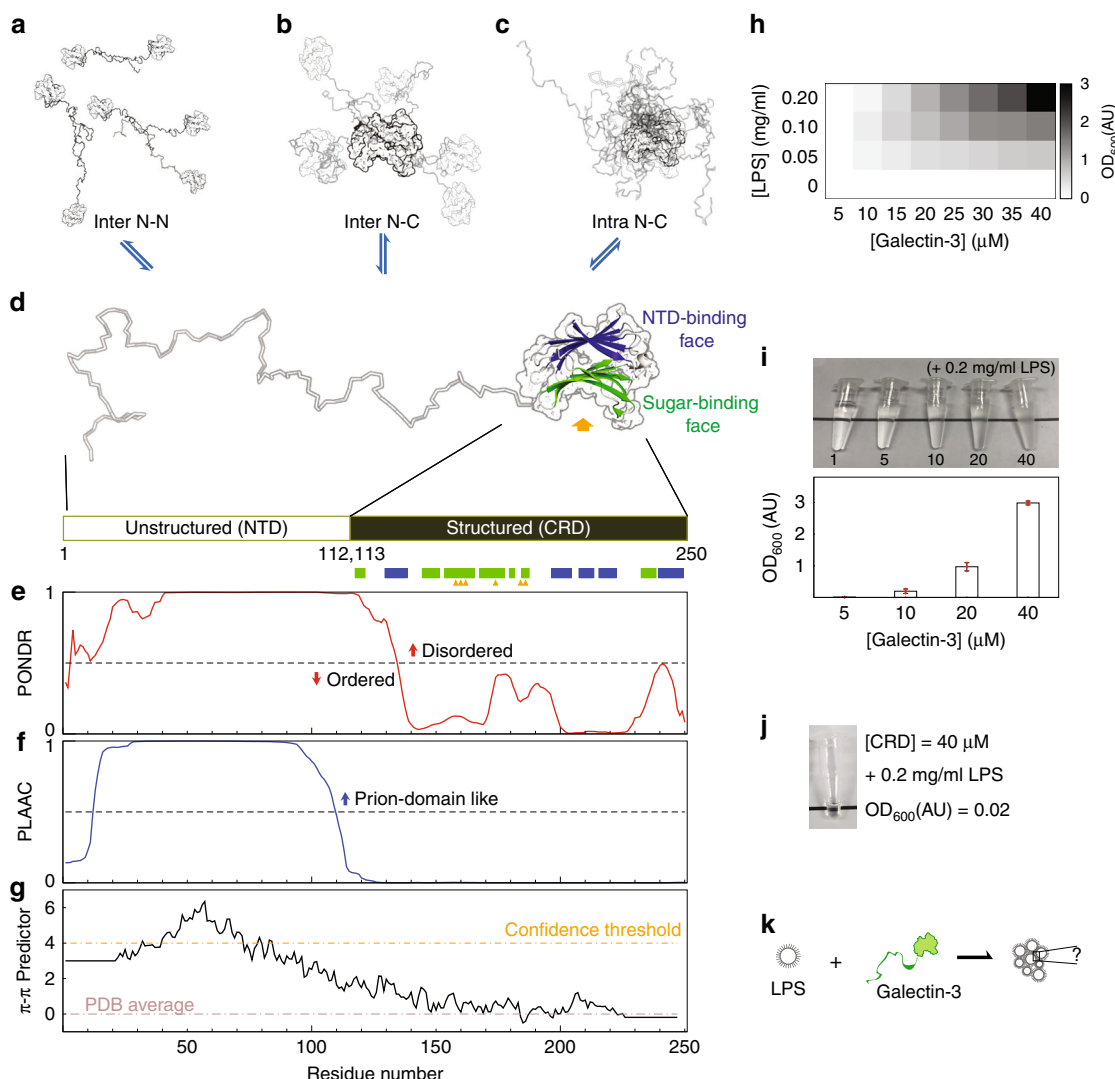
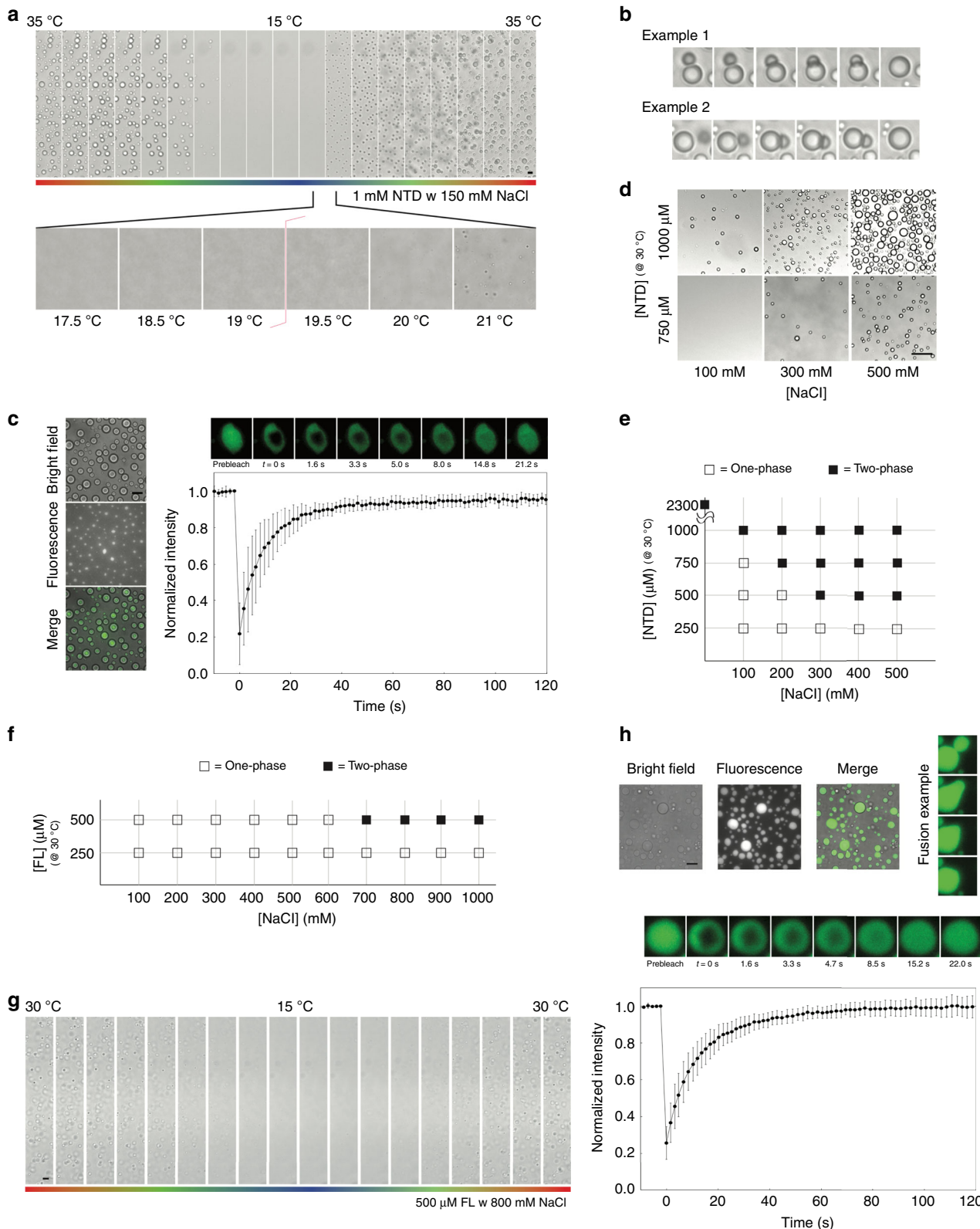


Fig. 1 Galectin-3 structure, sequence analysis and lipopolysaccharide (LPS) assay. **a, b** Intermolecular and **(c)** intramolecular galectin-3 interactions identified in a previous study. **d** A galectin-3 monomer: the structured carbohydrate recognition domain is represented by the solved crystal structure (PDB code, 2NMO), with the (non-canonical) N-terminal domain (NTD)-interaction face (with five β -strands) colored blue and the (canonical) sugar binding face (with six β -strands) colored green. Sugar-specific binding sites are indicated with yellow arrows. **e–g** Sequence analyses: **(e)** level of structural disorder (using PONDR⁷⁹), **(f)** similarity to prion-like proteins (using PLAAC)⁵³, **(g)** propensity to form π - π interactions⁵⁴. **h, i** Turbidity ($\text{OD}_{600\text{nm}}$) of LPS-galectin-3 samples measured at different protein and LPS concentrations. **j** Photograph of the CRD-only sample under the maximum turbidity conditions in panel **i**. **k** A schematic illustration of the main question of this study: what drives monomeric galectin-3 to agglutinate?

even more highly among mammals (Supplementary Fig. 3). Although the sequences of the intrinsically disordered regions are not similar, two patterns are conserved: proline-glycine repeats followed by aromatic residues (PGxY or PGxW motifs) and a net negative charge. The fact that these patterns are conserved suggests that they are functionally important. The abundance of Tyr or Trp residues has been shown in RNA binding proteins to promote LLPS, such as tyrosines in hnRNP A2 and FUS⁵⁸ and tryptophans in TDP-43 (ref. ⁵⁹). On this basis, we characterized the self-association tendency of three constructs in which all tryptophans, all tyrosines, or all tryptophans and tyrosines were replaced with glycines (denoted W/G, Y/G, and WY/G, respectively; Fig. 3b).

We showed in a previous study that intermolecular NTD interactions are negligible at protein concentrations lower than 40 μM , but pronounced at 400 μM ⁵⁰ (in the single-phase regime). We therefore compared the NMR peak intensities of 40 and 400 μM NTD samples in the absence of salt. The I_{40}/I_{400} peak

intensity ratios (Fig. 3c) are higher than the corresponding molar ratio (0.1), indicating that the signals in the spectra from the 400 μM are broader, presumably because of self-association. The average ratio increases with temperature, suggesting that this self-association is driven by hydrophobicity⁶⁰. We did not apply the NMR studies on the sample in the heterogeneous state because the size of the condensate was too large for NMR detection and thus we cannot differentiate that the signal loss is because of forming higher-order oligomers or self-association. Furthermore, high salt concentration also deteriorates the quality of NMR spectrum. For the W/G and Y/G constructs, the intensity ratios are closer to the molar ratio and when all tryptophan and tyrosine residues are removed (WY/G), the intensity ratios are the same as the molar ratio and independent of temperature (Fig. 3c). In agreement with the intensity ratio results, the transverse relaxation rate constants (R_2), which reflect the overall effects of tumbling, the internal motions of the molecule, and chemical exchange due to micro-to-millisecond



timescale motion^{61,62}, are concentration dependent for the wild-type NTD, indicating intermolecular association at the higher concentration, but not for the WY/G construct (Fig. 3d). (As demonstrated previously⁵⁰, the longitudinal relaxation rate constants, R_1 , do not vary with the concentration.) For the other constructs, the overall reduction in R_2 (cf. the black lines in Fig. 3d and Supplementary Fig. 4c) indicates increased dynamics

and flexibility (Supplementary Fig. 4b). We mapped the NMR chemical shift assignments of the wild-type and the W/G construct based on a previous publication⁶³. We did not assign the chemical shifts of the Y/G and WY/G constructs (marked as unassigned in Fig. 3) because only the overall trend in the peak intensity ratios and R_2 changes are critical to our interpretation. Furthermore, severe overlap in the NMR spectra of these two

Fig. 2 Micrographs illustrating the liquid-liquid phase separation (LLPS) properties. a-e the N-terminal domain (NTD); **(f-h)** full-length galectin-3. **a** A 1 mM sample with 150 mM NaCl condensing reversibly as a function of temperature (35–15–35 °C; scale bar: 10 µm), **b** Examples of condensate fusion. Experiments were performed at least three times for each protein sample. **c** Bright field and fluorescence micrographs alongside the results of fluorescence recovery after photobleaching (FRAP) experiments (scale bar: 50 µm; FRAP recovery curve is averaged from 10 different condensates; data are presented as mean values \pm SD). **d** Examples of the effects on condensate formation of the protein and salt concentrations (scale bar: 50 µm) and **(e)** the corresponding phase diagram (at a fixed temperature of 30 °C). Experiments were performed at least three times for each protein sample. **f** Phase diagram of full-length galectin-3 as the function of protein and salt concentration. **g** Micrographs showing a 500 µM full-length galectin-3 sample with 800 mM NaCl condensing reversibly as a function of temperature (30–15–30 °C; scale bar: 10 µm). Experiments were performed at least three times for each protein sample. **h** Bright field and fluorescence micrographs alongside the results of FRAP experiments with an example of condensate fusion (scale bar: 50 µm; FRAP recovery curve is averaged from 10 different condensates; data are presented as mean values \pm SD).

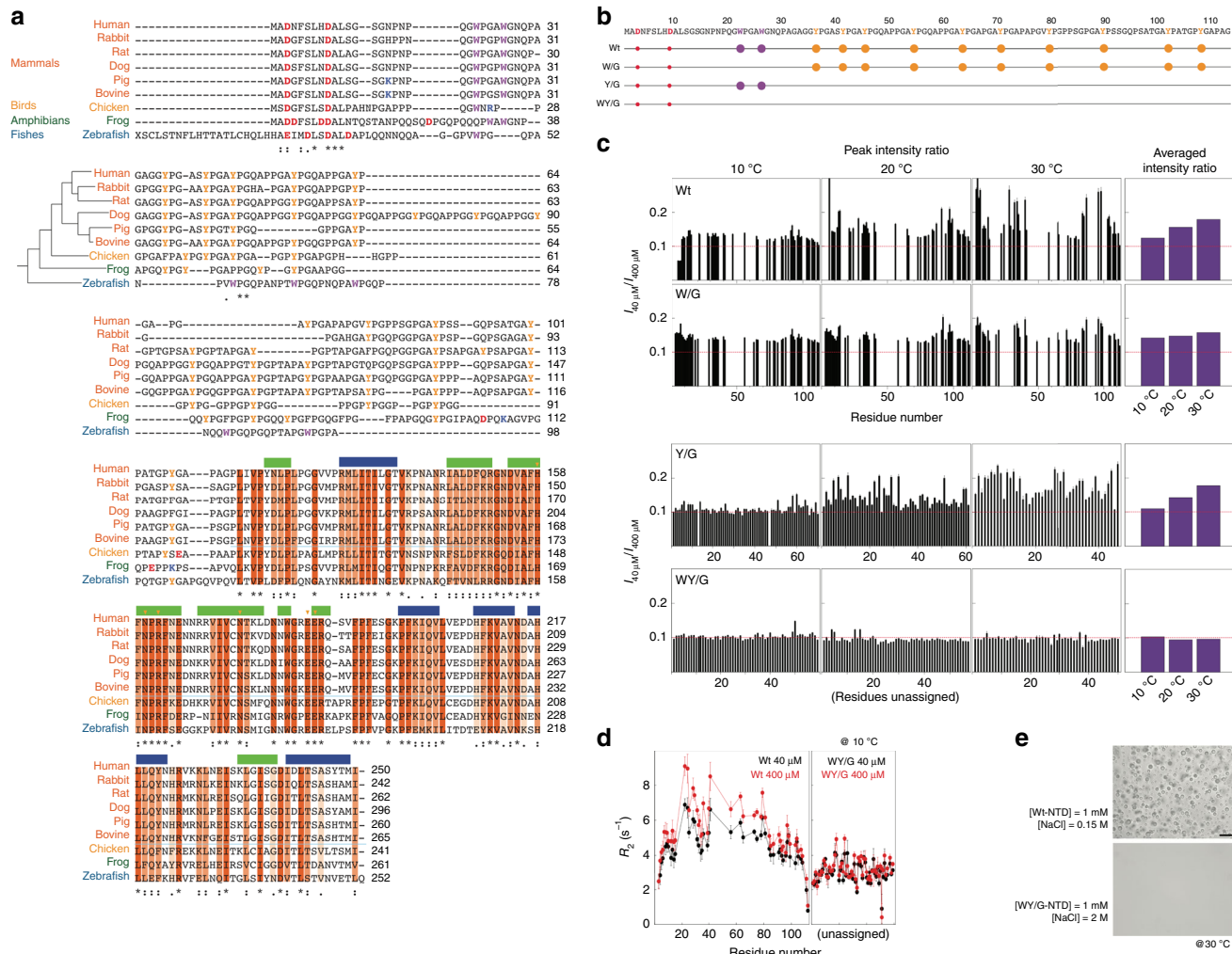


Fig. 3 The key residues that mediate intermolecular N-terminal domain (NTD) interactions. a Alignment of galectin-3 amino-acid sequences from different vertebrates (human, five mammals, one bird, one amphibian, and one fish). The phylogenetic tree is plotted based on a summary of multigene and multiprotein studies⁸⁷. Residues in the carbohydrate recognition domain (CRD) are highlighted with dark, medium, or light orange depending on their level of conservation. Negatively and positively charged residues, tyrosines, and tryptophans in the NTD are colored in red, blue, yellow and purple, respectively. **b** Amino-acid sequences of the constructs used in this study with negatively charged residues, tryptophans, and tyrosines highlighted by solid red, purple, and yellow circles, respectively. **c** NMR peak intensity ratios between 40 and 400 µM samples at 10, 20, and 30 °C for the four NTD constructs. The average peak intensity ratios at each temperature are shown in the right-most panel. Red dashed lines indicate the intensity ratio expected from the molar ratio (0.1). **d** Transverse relaxation rate constants for the 40 (black) and 400 (red) µM wild-type and W/Y/G mutants at 10 °C. **e** Micrographs of samples of wild-type galectin-3 and the W/Y/G construct under conditions corresponding to the two-phase regime in the wild-type phase diagram (Fig. 2e; scale bar: 50 µm). Experiments were performed at least three times for each protein sample.

constructs (because of the many repeated amino-acid motifs) would have made assignment difficult. Overlapping peaks also provide limited residue-specific information. In these constructs, we therefore only analyzed the well-resolved peaks to avoid bias due to peak overlap.

The reduction in intermolecular self-association indeed abolishes phase separation. At a concentration of 1 mM, the wild-type NTD enters the two-phase regime at salt concentrations above 0.1 M at 30 °C (Fig. 2e) whereas condensates were only observed for the W/Y/G construct when the NaCl concentration was

2 M (Supplementary Fig. 5). However, even at such a high NaCl concentration, the WY/G construct remains single phase (Fig. 3e). These results indicate that NTD monomers assemble through intermolecular interactions involving aromatic residues.

The importance of aromatic residues in full-length galectin-3. The intermolecular and intramolecular interactions between the NTD and the CRD can be distinguished using NMR peaks from the non-carbohydrate-binding site (colored blue in Fig. 1d; NMR spectra in Fig. 4d): The chemical shift differences between the CRD-only and full-length constructs indicate that the NTD and CRD interact intramolecularly via the non-carbohydrate-binding site (blue arrows in Fig. 4d; schematic representation on the right). The concentration-dependent chemical shift perturbations in the non-carbohydrate-binding site for wild-type galectin-3 indicate that the NTD and CRD also interact intermolecularly (orange arrows in Fig. 4d; see ref. 50 for more details). Compared with the wild type, intermolecular and intramolecular NTD-CRD interactions are weaker in the W/G mutant (Fig. 4a; comparison with wild-type spectra in Supplementary Fig. 6a) and more obviously so in the Y/G mutant (Fig. 4b), indicating that the two remaining tryptophans and the ten remaining tyrosines contribute to self-association. The relative contributions of the two types of aromatic residues cannot be evaluated because their numbers differ. The NMR peaks from the 40 and 400 μ M full-length WY/G mutant all overlap, indicating that there is no self-association (Fig. 4c, e). Note also that the peaks from the CRD in the full-length WY/G construct overlap with the corresponding peaks in the CRD-only spectrum (Fig. 4c), indicating that the NTD and the CRD do not interact. The R_2 s of the full-length WY/G construct are likewise similar at the two concentrations, in contrast with the wild type (Fig. 4f, h), leading to the same conclusion. Furthermore, the average R_2 is lower when the aromatic residues are removed, indicating increased motion in the protein, presumably because there is less chemical exchange driven by intermolecular and intramolecular interactions (Fig. 4f, h and Supplementary Fig. 6b, c). Although the aromatic residues do not contribute to the constructs' level of disorder and prion-likeness (Supplementary Fig. 7), the loss of them reduces their predicted propensity to form π - π interactions (Fig. 4i). Removal of the aromatic residues also prevents LLPS in full-length samples. No condensates were observed for the 500 μ M WY/G construct with 1 M NaCl at 30 °C (Fig. 4j), conditions under which the wild-type sample is in the two-phase regime (Fig. 2f).

Multivalent connections in galectin-3/micelle agglutination. Samples of full-length galectin-3 and of the NTD alone become heterogeneous at non-physiological protein or NaCl concentrations (Fig. 2). However, the function studied here is galectin-3's ability to agglutinate. Galectin-3 binding on the surface of LPS micelles increases the local protein concentration to levels in the tens of mM range (see estimate in the Supplementary Note 1), much higher than in the samples prepared here. The fact that the NTD and the full-length construct undergo LLPS suggests that multivalent crosslinking contributes to galectin-3's agglutination function. Just as we did for full-length galectin-3 (Fig. 1i), we used LPS micelle assays to investigate agglutination in the galectin-3 constructs: the full-length W/G mutant also became turbid but to a lesser extent, but the CRD-only, NTD-only, full-length Y/G and WY/G samples remained transparent when mixed with LPS (Fig. 5a, b; Supplementary Table 3; adding NaCl had little effect on the turbidity of the samples, Supplementary Fig. 8a).

The NMR peak intensities with and without LPS for the full-length wild type and the NTD-only, CRD-only, and full-length WY/G constructs (40 μ M samples with 0.2 mg/ml LPS) are

compared in Supplementary Fig. 8b. For the full-length wild type, the signal intensity in the presence of LPS was too weak for further analysis (Supplementary Fig. 8b, the only signals detected were from the flexible NTD domain) because the large size of the protein-micelle aggregates leads to severe line broadening. Although the NTD-only, CRD-only, and WY/G constructs remained transparent when mixed with LPS (Fig. 5a), different intensity ratio distributions were measured for the three samples (Fig. 5c). For the NTD-only construct, the fact that the peak intensity ratios are all about 1 indicates that there is no interaction with the micelles (Fig. 5c, d). The significantly lower peak intensities in the presence of LPS for the CRD-only construct (Fig. 5c) can be explained by a substantial proportion of the molecules binding to the polysaccharides of LPS and thus those CRDs' NMR signal is undetectable because of the reduced overall tumbling rate of the protein on the large LPS micelles (Fig. 5d). The same mechanism explains why the peaks from the CRD in the WY/G mutant decrease in intensity in the presence of LPS (Fig. 5c), but those from the NTD do not, as the CRD interacts with LPS while the NTD remains highly dynamic (Fig. 5d). Figure 5e shows the model proposed on the basis of these results for the interaction between full-length wild-type galectin-3 and LPS. When LPS micelles loaded with galectin-3 come into contact, the NTDs interact through their aromatic residues (the mechanism that drives LLPS in the absence of LPS; Fig. 2), leading to agglutination, as depicted in Fig. 5e. The turbidity of the LPS/galectin-3 mixtures is proportional to the protein concentration (Fig. 1h), which is consistent with this velcro-like behavior of the NTD: the more galectin-3 molecules are attached to each micelle, the more they tend to agglutinate.

Adding 25 mM lactose, a commonly used ligand for galectin-3, dissolves the galectin-3-LPS mixture (40 μ M and 0.2 mg ml⁻¹, respectively; Fig. 6a). The NMR spectrum of this sample has peaks of the same intensity and at the same chemical shifts as that of the same concentration of galectin-3 and lactose without LPS (Fig. 6b, c), indicating that galectin-3 returns to the monomeric state even after having agglutinated LPS. The chemical shift changes in the residues around the carbohydrate-binding face confirm the binding of lactose (Fig. 6d). Our results indicate that the NTD remains highly dynamic at all stages of the process and that the interactions are transient (Fig. 6e). When the CRD is bound to LPS, this increases the local protein concentration and the transient interactions between the NTDs promote agglutination. When the interaction between the CRD and LPS is blocked by lactose, the local concentration is too low to maintain the interactions between the NTDs and the protein molecules return to their monomeric state (Fig. 6e). We cannot rule out the possibility that interactions between lactose and the CRD also cause a conformational change that reduces the propensity to phase separate as there were chemical shift perturbations in the non-carbohydrate-binding site (Fig. 6d). These lactose experiments indicate that unlike the other members of the galectin family, which form dimers or are tandem repeats, free galectin-3 is monomeric in solution, without preformed oligomers.

Discussion

The functional repertoire of biomolecular condensates has only recently begun to come to light⁵⁵. This repertoire is not limited to intracellular functions however. LLPS is thought to initiate the assembly of many proteins in the extracellular matrix⁶⁴, as studied using model peptides designed to mimic elastins⁶⁵. The intrinsically disordered NTD of galectin-3 has many repeated proline-glycine motifs, which are also found in elastin-like proteins. However, the prevalence of aromatic residues in the NTD is not typical of elastins but of proteins known to undergo LLPS.

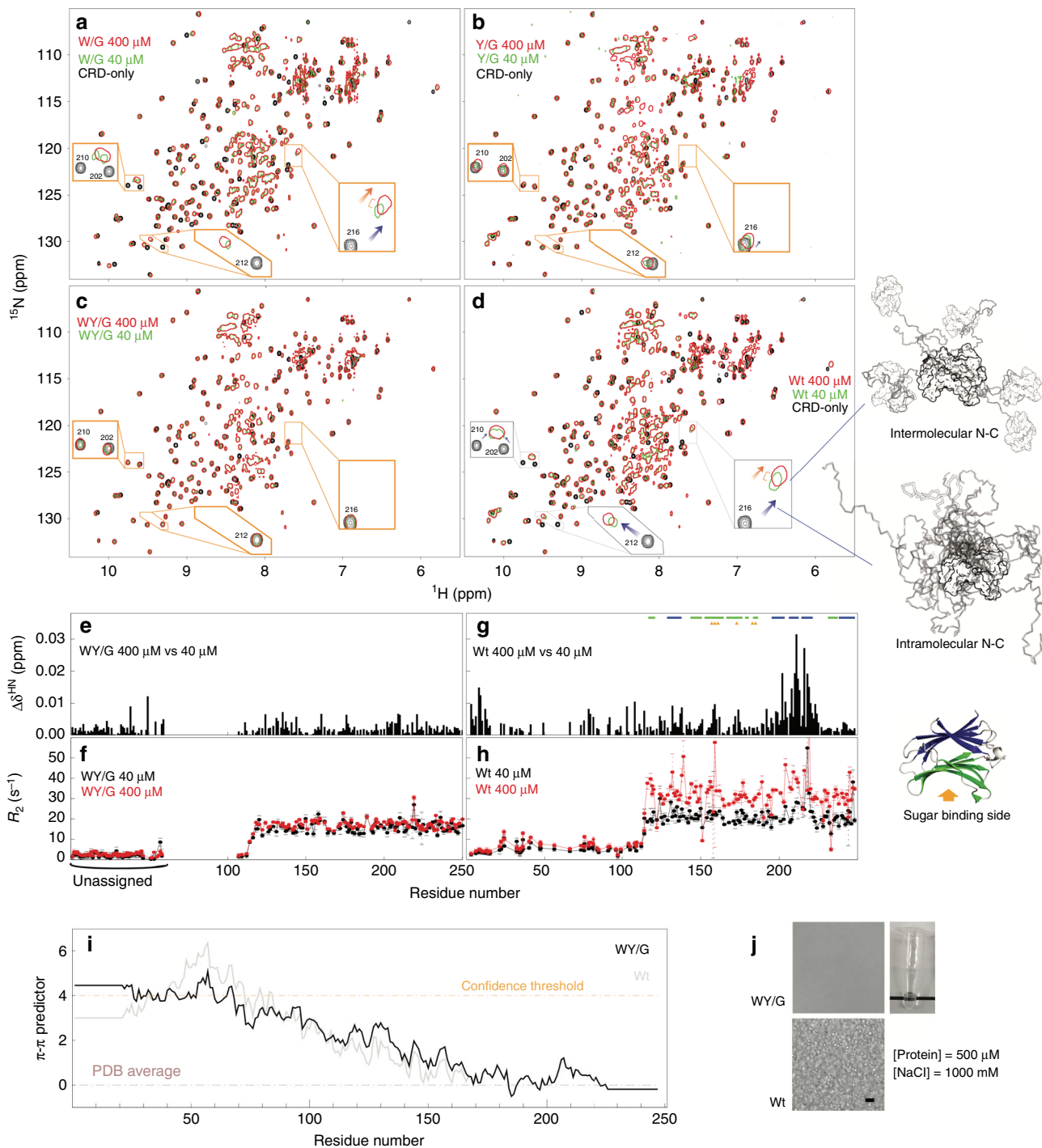


Fig. 4 Intermolecular and intramolecular interactions and liquid-liquid phase separation in full-length galectin-3. **a-d** NMR spectra of 400 (red) and 40 (green) μM samples of the four full-length constructs of galectin-3 compared to those from the CRD-only construct (black, 400 μM). Expanded views are shown of the regions in which the peaks shift the most. Blue arrows indicate chemical shift differences due to intramolecular NTD-CRD interactions (full-length spectra vs. the CRD-only spectrum); orange arrows indicate chemical shift differences due to intermolecular NTD-CRD interactions (400 vs. 40 μM spectra). Schematic illustrations of these interactions are shown on the right of the figure. **e, g** Chemical shift and **(f, h)** transverse relaxation rate constant differences between 400 and 40 μM samples for the WY/G mutant and the wild type. **i** Propensity to form π - π interactions of the WY/G construct. **j** Photograph and micrographs (scale bar: 10 μm) of samples of the full-length galectin-3 variants under conditions corresponding to the two-phase regime of the phase diagram of full-length wild-type galectin-3 (Fig. 2f). Experiments were performed at least three times for each protein sample.

Furthermore, while positively charged lysines (responsible for covalent crosslinking) are prevalent in elastin-like proteins, there are few charged residues in galectin-3's NTD, with a net negative charge in all vertebrates (Fig. 3a), suggesting that the NTD, although disordered, serves a function. Our data (Fig. 2) confirm

the propensity to assembly suggested by prion-likeness and π - π interaction sequence analysis, with the aromatic residues acting as “stickers”^{6,66} (Fig. 3). These weak contacts lead to the formation of stronger assemblies when the protein concentration (i.e. the number of stickers) is above the phase transition boundary. Our

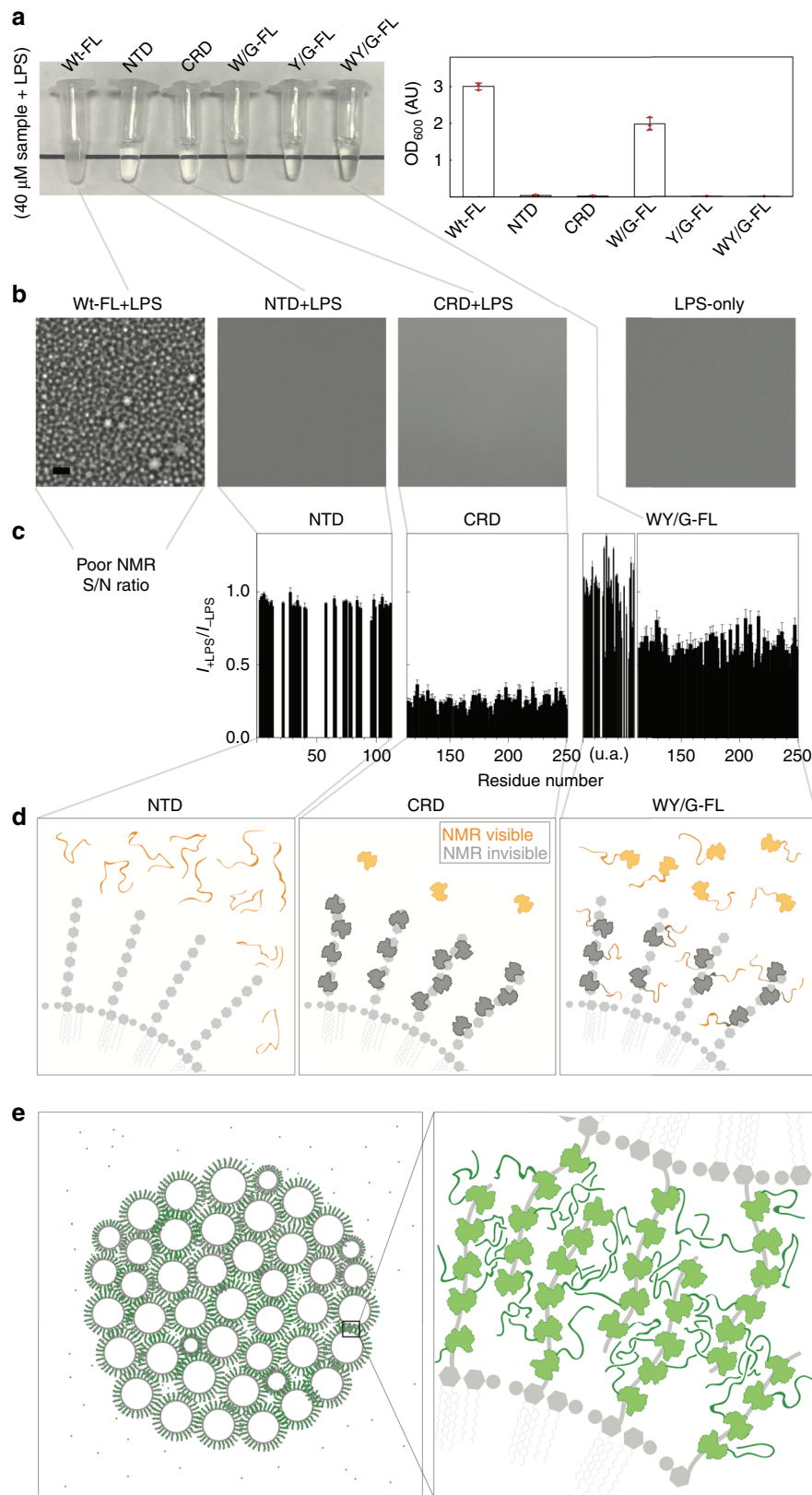


Fig. 5 Lipopolysaccharide (LPS) micelle agglutination assays. **a** Photograph and turbidity (OD₆₀₀) ($n = 3$ independent experiments; data are presented as mean values \pm SD) and **(b)** micrographs of samples of the different galectin-3 constructs in the presence of LPS. Experiments were performed at least three times for each protein sample (Scale bar: 10 μ m). **c** NMR peak intensity ratios in the presence and absence of LPS plotted as a function of residue number for the N-terminal domain (NTD)-only, carbohydrate-recognition domain (CRD)-only, and WY/G constructs. (This analysis was not possible for the full-length wild type because of a poor signal-to-noise ratio (Supplementary Fig. 8). **d** Schematic illustrations explaining the intensity changes for the NTD-only, CRD-only, and WY/G constructs. **e** Schematic illustration of the proposed mechanism of LPS-micelle agglutination driven by full-length wild-type galectin-3.

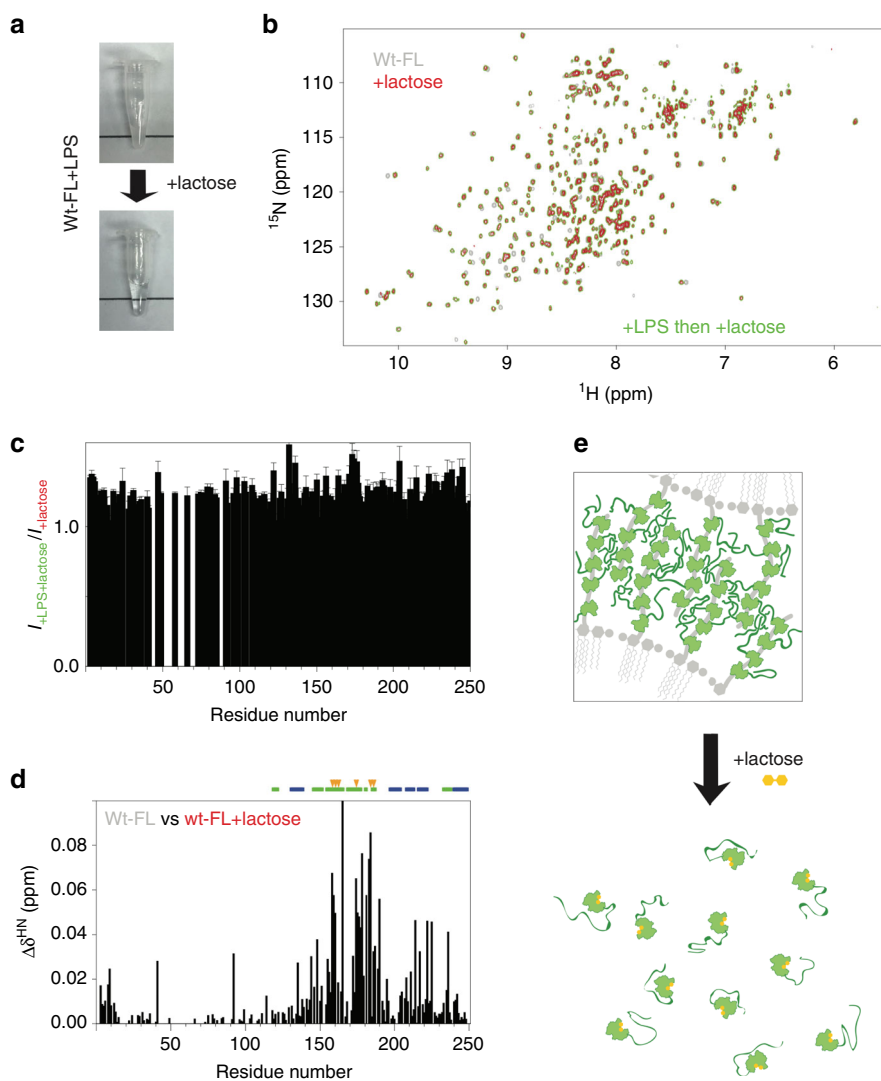


Fig. 6 Interaction with lactose inhibits galectin-3 agglutination. **a** Photographs of a galectin-3 (40 μ M) and LPS micelles (~0.2 mg ml $^{-1}$) sample before and after adding 25 mM lactose, which disrupts the aggregates. **b** Comparison of the spectra of 40 μ M samples of full-length wild type without LPS before (gray) and after adding 25 mM lactose (red), or mixed with LPS in the presence of 25 mM lactose (green). **c** NMR peak intensities of the LPS/galectin-3 sample recovered with 25 mM lactose normalized to the corresponding peak intensities from a sample of galectin-3 with the same amount of lactose but no LPS. **d** Chemical shift differences between the spectra recorded in the presence vs. in the absence of lactose (red (or green) vs. gray in panel **b**). The most pronounced changes in chemical shift occur for residues in the carbohydrate binding site (indicated with orange arrows) confirming the binding of lactose. **e** Illustration of how lactose dissolves the galectin-3/LPS aggregates.

analysis also shows that the aromatic residues also contribute to LLPS, intramolecular interactions, and (micelle) agglutination in full-length galectin-3 (Figs. 4, 5). In the model we propose (Figs. 5, 6), the CRD binds to surface glycans, exposing the NTD and promoting intermolecular interactions, which lead to the formation of micelle aggregates when the local concentration of NTDs is high enough to maintain strong connections. However, because the interactions are transient and dynamic, the protein-micelle aggregates return to the monomeric state when connections between the two are prevented (Fig. 6e). These results add an extracellular process to the functional repertoire⁵⁵ of LLPS.

LLPS can be artificially induced in some cases to demonstrate how the propensity to aggregate is related to function or disease, as shown for example in eye lens crystallins^{67,68} and in disease-related hemoglobin mutants⁶⁹. Although galectin-3 only undergoes LLPS under non-physiological conditions, it agglutinates in the extracellular matrix through interactions with cell surface

ligands that locally increase its concentration. This agglutination may involve the same multivalent mechanism as the one that drives LLPS and is reminiscent of the intrinsically disordered regions of nucleoporins (the FG-repeats), which are locally concentrated in the passage of the nuclear pore complex. This FG-repeat region is also regarded as a biomolecular condensate² and their phase properties have been studied⁷⁰. A similar effect is described in a recent study of the m⁶A-binding protein YTHDF⁷¹: YTHDF only functions when mRNA is poly-methylated such that many copies of YTHDF are recruited and the local concentration becomes high enough for the IDR to undergo LLPS. With singly methylated mRNA on the other hand, the single weakly bound YTHDF molecule does not undergo LLPS and is not functional. Our model is also consistent with known behaviors of galectin-3: in agreement with our turbidity vs. concentration results for example (Fig. 1i), galectin-3 adhesion increases with concentration in many types of inflammatory

cells³³. How an accumulation of weak interactions can lead to stronger cell-cell adhesion via the NTD is illustrated in Supplementary Fig. 9. Although many studies have shown that removing the NTD leads to loss of function^{33,37,47}, our model shows more specifically how LLPS is initiated by interactions between aromatic residues in the NTD. Galectin-3, unlike dimeric and tandem repeat galectins, may have evolved multivalency through an LLPS-like mechanism, with the potential advantage that agglutination depends on the amount of protein present in the extracellular milieu.

Fuzzy interactions also facilitate crosslinking between galectins and glycolipids or glycoproteins to form the glycan-galectin lattice, a component of many mechanisms such as the regulation of receptor kinases and inflammatory response⁷². Inserting our model into these molecular processes yields the following scenario: galectin-3 molecules attached to glycoproteins on membrane rafts come into contact by diffusion. When the galectin-3 concentration is low, the weak NTD-NTD interactions do not stabilize the glycan-galectin lattice; however, if enough galectin-3 molecules are attached, galectin-3 agglutinates the membrane glycoproteins, inducting⁷³ or inhibiting⁷⁴ downstream signaling (Supplementary Fig. 9b, c). Furthermore, the mechanism described here of how galectin-3 agglutinates is a potential target for drug design. Instead of designing compounds to selectively inhibit galectin-3's carbohydrate binding site (see ref. ⁷⁵ for example) rather than the CRDs of other members in the galectin family, targeting the aromatic residues in the NTD may also be a good strategy.

Our current study focuses on interpreting the extracellular function of galectin-3 but it seems probable that the NTD's ability to phase separate may also contribute to many of its intracellular functions, such as sensing danger by detecting unusual glycan exposure on damaged phagosomes⁷⁶ or by regulating RNA splicing⁷⁷ as do many RNA binding proteins with a prion-like domain (e.g., FUS, TDP-43). Moreover, many of the mechanisms governing the behavior of galectin-3 are still puzzling. For instance, how is the equilibrium between the N and C terminal domains (Fig. 1c vs. d) mediated? Does the level of negative charge play a role in the mediation of LLPS by phosphorylation (which adds more negative charge; phosphorylation sites have been identified⁷⁸)? Do galectin-3's interactions with binding partners through the non-canonical carbohydrate-binding site outcompete the NTD-CRD interaction and thereby release the NTD to regulate LLPS? It is evolutionarily unlikely that galectin-3's disordered tail is redundant and this article demonstrates how its multivalent interactions mediate function. Many mysteries about this chimeric protein remain and our study provides a framework for further investigations.

Methods

Sequence analysis. The level of structural disorder was predicted using the PONDR VLXT algorithm⁷⁹. Prion-likeness was predicted using the PLAAC algorithm⁵³ and $\pi-\pi$ interactions using the Pi-Pi prediction server (PScore Predictor)⁵⁴. The protein sequences were aligned using BLAST (www.uniprot.org/blast). The entries used to access the sequences from the database are listed in Supplementary Table 4.

DNA constructs. The cDNA of galectin-3 variants (full-length or NTD-only) was inserted into a pHD-vector containing a hexahistidine-tagged small ubiquitin-like modifier protein (His₆-SUMO) as described previously⁵⁰. The WY/G construct was created by whole gene synthesis (Supplementary Note 2). The primers used for the W/G (tryptophan changed to glycine on the wild-type template) and the Y/G (tryptophan changed glycine on the WY/G template) construct are listed in Supplementary Table 5. The cDNA of GFP was inserted at the C-terminus of the His₆-SUMO-NTD construct. All constructs were verified by DNA sequencing.

Protein expression and purification. All variants were purified using the same previously-described protocol⁵⁰. A fusion protein of hexahistidine, SUMO, and the

galectin-3 variant (His₆-SUMO-gal3v) was purified using a nickel-charged immobilized metal-ion affinity chromatography (IMAC) column (Qiagen, Inc.). The column was washed using 10 column volumes (CVs) of 50 mM Tris-HCl with 300 mM NaCl at pH 7.5, and the bonded-protein was eluted using five CVs of the same buffer with an additional 500 mM imidazole. Imidazole was removed using a PD-10 column (GE Healthcare, Inc.). 6xHis-Ulp1⁴⁰³⁻⁶²¹ protease was added to the protein solution with a final concentration of 30 μ M and left at 4 °C for 2 h to detach the 6xHis-SUMO tag and galectin-3. The protease-digested solution was loaded into a nickel-charged IMAC column, and the flow-through was collected. The target protein was concentrated using a Centricon centrifugal filter (Vivapure) and was exchanged with phosphate buffer (20 mM) at pH 6.8 using a PD-10 column (GE Healthcare). Protease inhibitor (Roche Applied Science) was added before storage. The purified NTD sample was flash frozen with liquid nitrogen and stored at -80 °C until needed. The full-length samples were stored at 4 °C for 2 days at most before experiments.

Microscopy. Micrographs were collected using an Olympus BX51 device equipped with a $\times 40$ long working distance objective. The images were recorded using a Zeiss AxioCam MRM camera. The protein samples were placed on a thermostatic stage (THM120, Linkam Scientific Inc.). The sample was equilibrated in this chamber for at least 3 min before each measurement.

Fluorescence recovery after photobleaching (FRAP) assays. Fluorescence recovery after photobleaching experiments on GFP-tagged proteins were performed using a 100 \times 1.49NA Plan objective lens attached to an *iLas* multimodal total internal reflection fluorescence (Roper)/spinning disk confocal (CSUX1, Yokogawa) microscope (Ti-E, Nikon). The stage temperature was maintained at 37 °C with an airstream incubator (Nevtek) and focus was maintained using the PerfectFocus^(TM) system (Nikon). The 488-nm laser was used to photobleach the fluorophores into a single fluorescent droplet. Images were acquired at 1 s intervals before and after photobleaching using an Evolve EMCCD camera (Photometrics) with an \sim 100 nm evanescent field depth. Images were captured and processed using the Metamorph software. Samples of NTD or full-length galectin-3 at 500 μ M in 500 mM or 1 M NaCl were mixed with 1% (5 μ M) of NTD-GFP or with 1% GFP as control.

NMR experiments and analysis. NMR data were collected on Bruker AVIII 850-MHz or 600-MHz spectrometers, both equipped with a TCI cryogenic probe. The ¹H-¹⁵N HSQC spectra and transverse relaxation rate experiments were collected using standard pulse sequences⁸⁰⁻⁸². In the dynamics experiments, the transverse relaxation rates were measured with delays of 17, 34, 51, 68 ms for the first four time points and 85 and 102 ms (for the full-length constructs) or 119 and 153 ms (for the NTD-only variants) for the last two. Peak intensities were fitted to exponential decays with a Monte Carlo procedure to estimate fitting error. The dynamics data were collected in an interleaved manner with an interscan delay of 3 s. All NMR data were collected at 30 °C, unless otherwise stated. The samples were prepared in 20 mM phosphate buffer at pH 6.8 containing protease inhibitor (Roche Applied Science) and 10% D₂O.

All data were processed using NMRPipe⁸³ and analyzed with SPARKY⁸⁴. Peak intensities and errors were determined using the non-linear line-shape analysis (nlinLS) function in NMRPipe based on the noise of the spectra. The intensity ratios were normalized to the number of scans and the errors were calculated using standard error propagation. The average chemical shift difference ($\Delta\delta^{\text{av}}$) was calculated using

$$\Delta\delta^{\text{av}} = \sqrt{\frac{(\Delta\delta_H)^2 + (\frac{1}{5}\Delta\delta_N)^2}{2}} \quad (1)$$

where $\Delta\delta_H$ and $\Delta\delta_N$ are the differences in chemical shift between two ¹H-¹⁵N HSQC spectra for the amide proton and nitrogen, respectively.

LPS assay. Lipopolysaccharide from *E. Coli* strain O55:B5 was purchased from Merck (Cat. L2880). A stock solution was prepared in 20 mM phosphate buffer at pH 6.8. The chosen amounts of LPS to be above the critical micelle concentration^{85,86} and protein solution were mixed directly before optical density or microscopy measurements. All measurements were performed in triplicate. For the NMR experiments comparing the behavior of galectin-3 with and without LPS, a batch of stock protein solution (at high concentration) was separated into two parts; LPS was added to one and the same volume of buffer to the other.

Reporting summary. Further information on experimental design is available in the Nature Research Reporting Summary linked to this paper.

Data availability

The source data underlying Figs. 1h, 1i, 2c, 2h, 3c, 3d, 4e-h, 5a, 5c, 6c, and 6d and Supplementary Figs. 4c, 6c, and 8a are provided as a Source Data file. Other data are available from the corresponding author upon reasonable request.

Received: 1 July 2019; Accepted: 15 February 2020;
Published online: 06 March 2020

References

- Warren, G. & Wickner, W. Organelle inheritance. *Cell* **84**, 395–400 (1996).
- Banani, S. F., Lee, H. O., Hyman, A. A. & Rosen, M. K. Biomolecular condensates: organizers of cellular biochemistry. *Nat. Rev. Mol. Cell Biol.* **18**, 285–298 (2017).
- Shin, Y. & Brangwynne, C. P. Liquid phase condensation in cell physiology and disease. *Science* **357** eaaf4382 (2017).
- Nott, T. J. et al. Phase transition of a disordered nuage protein generates environmentally responsive membraneless organelles. *Mol. Cell* **57**, 936–947 (2015).
- Hyman, A. A., Weber, C. A. & Julicher, F. Liquid-liquid phase separation in biology. *Annu. Rev. Cell Dev. Biol.* **30**, 39–58 (2014).
- Holehouse, A. S. & Pappu, R. V. Functional implications of intracellular phase transitions. *Biochemistry* **57**, 2415–2423 (2018).
- Kato, M. et al. Cell-free formation of RNA granules: low complexity sequence domains form dynamic fibers within hydrogels. *Cell* **149**, 753–767 (2012).
- Lin, Y., Trotter, D. S., Rosen, M. K. & Parker, R. Formation and maturation of phase-separated liquid droplets by RNA-binding proteins. *Mol. Cell* **60**, 208–219 (2015).
- Mollie, A. et al. Phase separation by low complexity domains promotes stress granule assembly and drives pathological fibrillization. *Cell* **163**, 123–133 (2015).
- Patel, A. et al. A liquid-to-solid phase transition of the ALS protein FUS accelerated by disease mutation. *Cell* **162**, 1066–1077 (2015).
- Qamar, S. et al. FUS phase separation is modulated by a molecular chaperone and methylation of arginine cation-pi interactions. *Cell* **173**, 720–734 e15 (2018).
- Hofweber, M. et al. Phase separation of FUS is suppressed by its nuclear import receptor and arginine methylation. *Cell* **173**, 706–719 e13 (2018).
- Lu, H. et al. Phase-separation mechanism for C-terminal hyperphosphorylation of RNA polymerase II. *Nature* **558**, 318–323 (2018).
- Boehning, M. et al. RNA polymerase II clustering through carboxy-terminal domain phase separation. *Nat. Struct. Mol. Biol.* **25**, 833–840 (2018).
- Hnisz, D., Shrinivas, K., Young, R. A., Chakraborty, A. K. & Sharp, P. A. A phase separation model for transcriptional control. *Cell* **169**, 13–23 (2017).
- Boija, A. et al. Transcription factors activate genes through the phase-separation capacity of their activation domains. *Cell* **175**, 1842–1855 e16 (2018).
- Sabari, B. R. et al. Coactivator condensation at super-enhancers links phase separation and gene control. *Science* **361**, eaar3958 (2018).
- Strom, A. R. et al. Phase separation drives heterochromatin domain formation. *Nature* **547**, 241–245 (2017).
- Larson, A. G. et al. Liquid droplet formation by HP1alpha suggests a role for phase separation in heterochromatin. *Nature* **547**, 236–240 (2017).
- Woodruff, J. B. et al. The centrosome is a selective condensate that nucleates microtubules by concentrating tubulin. *Cell* **169**, 1066–1077 e10 (2017).
- Rai, A. K., Chen, J. X., Selbach, M. & Pelkmans, L. Kinase-controlled phase transition of membraneless organelles in mitosis. *Nature* **559**, 211–216 (2018).
- Milovanovic, D., Wu, Y., Bian, X. & De Camilli, P. A liquid phase of synapsin and lipid vesicles. *Science* **361**, 604–607 (2018).
- Wu, X. et al. RIM and RIM-BP form presynaptic active-zone-like condensates via phase separation. *Mol. Cell* **73**, 971–984 e5 (2019).
- Zhang, G., Wang, Z., Du, Z. & Zhang, H. mTOR regulates phase separation of PGL granules to modulate their autophagic degradation. *Cell* **174**, 1492–1506 e22 (2018).
- Bouchard, J. J. et al. Cancer mutations of the tumor suppressor SPOP disrupt the formation of active, phase-separated compartments. *Mol. Cell* **72**, 19–36 e8 (2018).
- Frey, S. et al. Surface properties determining passage rates of proteins through nuclear pores. *Cell* **174**, 202–217 e9 (2018).
- Miles, S. et al. Plasticity of an ultrafast interaction between nucleoporins and nuclear transport receptors. *Cell* **163**, 734–745 (2015).
- Dao, T. P. et al. Ubiquitin modulates liquid-liquid phase separation of UBQLN2 via disruption of multivalent interactions. *Mol. Cell* **69**, 965–978 e6 (2018).
- Li, P. et al. Phase transitions in the assembly of multivalent signalling proteins. *Nature* **483**, 336–340 (2012).
- Su, X. et al. Phase separation of signaling molecules promotes T cell receptor signal transduction. *Science* **352**, 595–599 (2016).
- Taylor, M. E., Drickamer, K., Schnaar, R. L., Etzler, M. E. & Varki, A. Discovery and Classification of Glycan-Binding Proteins. in *Essentials of Glycobiology* 361–372 (Cold Spring Harbor, 2015).
- Cummings, R. D., Liu, F. T. & Vasta, G. R. Galectins. in *Essentials of Glycobiology* 469–480 (Cold Spring Harbor, 2015).
- Kuwabara, I. & Liu, F. T. Galectin-3 promotes adhesion of human neutrophils to laminin. *J. Immunol.* **156**, 3939–3944 (1996).
- Sato, S. et al. Role of galectin-3 as an adhesion molecule for neutrophil extravasation during streptococcal pneumonia. *J. Immunol.* **168**, 1813–1822 (2002).
- Lau, K. S. et al. Complex N-glycan number and degree of branching cooperate to regulate cell proliferation and differentiation. *Cell* **129**, 123–134 (2007).
- Goetz, J. G. et al. Concerted regulation of focal adhesion dynamics by galectin-3 and tyrosine-phosphorylated caveolin-1. *J. Cell Biol.* **180**, 1261–1275 (2008).
- Nieminen, J., Kuno, A., Hirabayashi, J. & Sato, S. Visualization of galectin-3 oligomerization on the surface of neutrophils and endothelial cells using fluorescence resonance energy transfer. *J. Biol. Chem.* **282**, 1374–1383 (2007).
- Friedrichs, J., Manninen, A., Muller, D. J. & Helenius, J. Galectin-3 regulates integrin alpha2beta1-mediated adhesion to collagen-I and -IV. *J. Biol. Chem.* **283**, 32264–32272 (2008).
- Ahmad, N. et al. Galectin-3 precipitates as a pentamer with synthetic multivalent carbohydrates and forms heterogeneous cross-linked complexes. *J. Biol. Chem.* **279**, 10841–10847 (2004).
- Fermino, M. L. et al. LPS-induced galectin-3 oligomerization results in enhancement of neutrophil activation. *PLoS ONE* **6**, e26004 (2011).
- Halimi, H. et al. Glycan dependence of Galectin-3 self-association properties. *PLoS ONE* **9**, e111836 (2014).
- Massa, S. M., Cooper, D. N., Leffler, H. & Barondes, S. H. L-29, an endogenous lectin, binds to glycoconjugate ligands with positive cooperativity. *Biochemistry* **32**, 260–267 (1993).
- Kukliniski, S. & Probstmeier, R. Homophilic binding properties of galectin-3: involvement of the carbohydrate recognition domain. *J. Neurochem.* **70**, 814–823 (1998).
- Lepur, A., Salomonsson, E., Nilsson, U. J. & Leffler, H. Ligand induced galectin-3 protein self-association. *J. Biol. Chem.* **287**, 21751–21756 (2012).
- Yang, R. Y., Hill, P. N., Hsu, D. K. & Liu, F. T. Role of the carboxyl-terminal lectin domain in self-association of galectin-3. *Biochemistry* **37**, 4086–4092 (1998).
- Ippel, H. et al. Intra- and intermolecular interactions of human galectin-3: assessment by full-assignment-based NMR. *Glycobiology* **26**, 888–903 (2016).
- Hsu, D. K., Zuberi, R. I. & Liu, F. T. Biochemical and biophysical characterization of human recombinant IgE-binding protein, an S-type animal lectin. *J. Biol. Chem.* **267**, 14167–14174 (1992).
- Morris, S. et al. Quaternary solution structures of galectins-1, -3, and -7. *Glycobiology* **14**, 293–300 (2004).
- Roff, C. F. & Wang, J. L. Endogenous lectins from cultured cells. Isolation and characterization of carbohydrate-binding proteins from 3T3 fibroblasts. *J. Biol. Chem.* **258**, 10657–10663 (1983).
- Lin, Y. H. et al. The intrinsically disordered N-terminal domain of galectin-3 dynamically mediates multisite self-association of the protein through fuzzy interactions. *J. Biol. Chem.* **292**, 17845–17856 (2017).
- Wu, H. & Fuxreiter, M. The structure and dynamics of higher-order assemblies: amyloids, signalosomes, and granules. *Cell* **165**, 1055–1066 (2016).
- Li, Y. et al. Galectin-3 is a negative regulator of lipopolysaccharide-mediated inflammation. *J. Immunol.* **181**, 2781–2789 (2008).
- Lancaster, A. K., Nutter-Upham, A., Lindquist, S. & King, O. D. PLAAC: a web and command-line application to identify proteins with prion-like amino acid composition. *Bioinformatics* **30**, 2501–2502 (2014).
- Vernon, R. M. et al. Pi-Pi contacts are an overlooked protein feature relevant to phase separation. *Elife* **7**, e31486 (2018).
- Alberti, S., Gladfelter, A. & Mittag, T. Considerations and challenges in studying liquid-liquid phase separation and biomolecular condensates. *Cell* **176**, 419–434 (2019).
- Posey, A. E., Holehouse, A. S. & Pappu, R. V. Phase separation of intrinsically disordered proteins. *Methods Enzymol.* **611**, 1–30 (2018).
- Ruff, K. M., Roberts, S., Chilkoti, A. & Pappu, R. V. Advances in understanding stimulus-responsive phase behavior of intrinsically disordered protein polymers. *J. Mol. Biol.* **430**, 4619–4635 (2018).
- Lin, Y., Currie, S. L. & Rosen, M. K. Intrinsically disordered sequences enable modulation of protein phase separation through distributed tyrosine motifs. *J. Biol. Chem.* **430**, 4741–4753 (2017).
- Li, H. R., Chiang, W. C., Chou, P. C., Wang, W. J. & Huang, J. R. TAR DNA-binding protein 43 (TDP-43) liquid-liquid phase separation is mediated by just a few aromatic residues. *J. Biol. Chem.* **293**, 6090–6098 (2018).
- Chandler, D. Interfaces and the driving force of hydrophobic assembly. *Nature* **437**, 640–647 (2005).
- Kay, L. E., Torchia, D. A. & Bax, A. Backbone dynamics of proteins as studied by 15N inverse detected heteronuclear NMR spectroscopy: application to staphylococcal nuclease. *Biochemistry* **28**, 8972–8979 (1989).
- Akke, M. Conformational dynamics and thermodynamics of protein-ligand binding studied by NMR relaxation. *Biochem. Soc. Trans.* **40**, 419–423 (2012).

63. Ippel, H. et al. (1)H, (13)C, and (15)N backbone and side-chain chemical shift assignments for the 36 proline-containing, full length 29 kDa human chimera-type galectin-3. *Biomol. NMR Assign.* **9**, 59–63 (2015).

64. Muiznieks, L. D., Sharpe, S., Pomes, R. & Keeley, F. W. Role of liquid-liquid phase separation in assembly of elastin and other extracellular matrix proteins. *J. Mol. Biol.* **430**, 4741–4753 (2018).

65. Reichheld, S. E., Muiznieks, L. D., Keeley, F. W. & Sharpe, S. Direct observation of structure and dynamics during phase separation of an elastomeric protein. *Proc. Natl Acad. Sci. USA* **114**, E4408–E4415 (2017).

66. Wang, J. et al. A molecular grammar governing the driving forces for phase separation of prion-like RNA binding proteins. *Cell* **174**, 688–699 e16 (2018).

67. Broide, M. L., Berland, C. R., Pande, J., Ogun, O. O. & Benedek, G. B. Binary-liquid phase separation of lens protein solutions. *Proc. Natl Acad. Sci. USA* **88**, 5660–5664 (1991).

68. Annunziata, O., Ogun, O. & Benedek, G. B. Observation of liquid-liquid phase separation for eye lens gammaS-crystallin. *Proc. Natl Acad. Sci. USA* **100**, 970–974 (2003).

69. Chen, Q., Vekilov, P. G., Nagel, R. L. & Hirsch, R. E. Liquid-liquid phase separation in hemoglobins: distinct aggregation mechanisms of the beta6 mutants. *Biophys. J.* **86**, 1702–1712 (2004).

70. Schmidt, H. B. & Gorlich, D. Transport selectivity of nuclear pores, phase separation, and membraneless organelles. *Trends Biochem. Sci.* **41**, 46–61 (2016).

71. Ries, R. J. et al. m(6)A enhances the phase separation potential of mRNA. *Nature* **571**, 424–428 (2019).

72. Nabi, I. R., Shankar, J. & Dennis, J. W. The galectin lattice at a glance. *J. Cell Sci.* **128**, 2213–2219 (2015).

73. Lagana, A. et al. Galectin binding to Mgat5-modified N-glycans regulates fibronectin matrix remodeling in tumor cells. *Mol. Cell Biol.* **26**, 3181–3193 (2006).

74. Demetriou, M., Granovsky, M., Quaggin, S. & Dennis, J. W. Negative regulation of T-cell activation and autoimmunity by Mgat5 N-glycosylation. *Nature* **409**, 733–739 (2001).

75. Stegmayer, J. et al. Extracellular and intracellular small-molecule galectin-3 inhibitors. *Sci. Rep.* **9**, 2186 (2019).

76. Weng, I. C. et al. Cytosolic galectin-3 and -8 regulate antibacterial autophagy through differential recognition of host glycans on damaged phagosomes. *Glycobiology* **28**, 392–405 (2018).

77. Dagher, S. F., Wang, J. L. & Patterson, R. J. Identification of galectin-3 as a factor in pre-mRNA splicing. *Proc. Natl Acad. Sci. USA* **92**, 1213–1217 (1995).

78. Huflejt, M. E., Turck, C. W., Lindstedt, R., Barondes, S. H. & Leffler, H. L-29, a soluble lactose-binding lectin, is phosphorylated on serine 6 and serine 12 in vivo and by casein kinase I. *J. Biol. Chem.* **268**, 26712–26718 (1993).

79. Romero, P. et al. Sequence complexity of disordered protein. *Proteins* **42**, 38–48 (2001).

80. Piotto, M., Saudek, V. & Sklenar, V. Gradient-tailored excitation for single-quantum NMR spectroscopy of aqueous solutions. *J. Biomol. NMR* **2**, 661–665 (1992).

81. Bodenhausen, G. & Ruben, D. J. Natural abundance N-15 NMR by enhanced heteronuclear spectroscopy. *Chem. Phys. Lett.* **69**, 185–189 (1980).

82. Farrow, N. A. et al. Backbone dynamics of a free and phosphopeptide-complexed Src homology 2 domain studied by 15N NMR relaxation. *Biochemistry* **33**, 5984–6003 (1994).

83. Delaglio, F. et al. NMRPipe: a multidimensional spectral processing system based on UNIX pipes. *J. Biomol. NMR* **6**, 277–293 (1995).

84. Goddard, T. D. & Kneller, D. G. *Sparky 3*. (University of California, San Francisco, 2005).

85. Santos, N. C., Silva, A. C., Castanho, M. A., Martins-Silva, J. & Saldanha, C. Evaluation of lipopolysaccharide aggregation by light scattering spectroscopy. *Chembiochem* **4**, 96–100 (2003).

86. Yu, L., Tan, M., Ho, B., Ding, J. L. & Wohland, T. Determination of critical micelle concentrations and aggregation numbers by fluorescence correlation spectroscopy: aggregation of a lipopolysaccharide. *Anal. Chim. Acta* **556**, 216–225 (2006).

87. Hedges, S. B. The origin and evolution of model organisms. *Nat. Rev. Genet.* **3**, 838–849 (2002).

Acknowledgements

The authors thank Prof. Won-Jing Wang (NYMU) for access to the microscope, Prof. Fu-Tong Liu (Academia Sinica) for helpful comments, and the Core Facility for Protein Structural Analysis in Academia Sinica for access to the NMR spectrometers. This work was supported by the Ministry of Science and Technology of Taiwan (106-2113-M-010-005-MY2 and 108-2113-M-010-005).

Author contributions

J.R.H. conceived the project and wrote the paper. Y.P.C., Y.C.S., D.C.Q., Y.H.L., and J.R.H. designed the experiments. Y.P.C., Y.C.S., D.C.Q., Y.H.L., Y.Q.C., J.C.K., and J.R.H. collected and analyzed the data.

Competing interests

The authors declare no competing interests.

Additional information

Supplementary information is available for this paper at <https://doi.org/10.1038/s41467-020-15007-3>.

Correspondence and requests for materials should be addressed to J.-R.H.

Peer review information *Nature Communications* thanks the anonymous reviewer(s) for their contribution to the peer review of this work. Peer reviewer reports are available.

Reprints and permission information is available at <http://www.nature.com/reprints>

Publisher's note Springer Nature remains neutral with regard to jurisdictional claims in published maps and institutional affiliations.



Open Access This article is licensed under a Creative Commons Attribution 4.0 International License, which permits use, sharing, adaptation, distribution and reproduction in any medium or format, as long as you give appropriate credit to the original author(s) and the source, provide a link to the Creative Commons license, and indicate if changes were made. The images or other third party material in this article are included in the article's Creative Commons license, unless indicated otherwise in a credit line to the material. If material is not included in the article's Creative Commons license and your intended use is not permitted by statutory regulation or exceeds the permitted use, you will need to obtain permission directly from the copyright holder. To view a copy of this license, visit <http://creativecommons.org/licenses/by/4.0/>.

© The Author(s) 2020

Supplementary Information

Liquid-liquid phase separation and extracellular multivalent interactions in the tale of galectin-3

Y.-P. Chiu, Y.-C. Sun et al.

Supplementary Table 1. O.D₆₀₀ (A.U.) for Fig. 1h.

		Galectin-3 (μM)							
		5	10	15	20	25	30	35	40
LPS (mg/ml)	0.2	0.01	0.196	0.523	0.969	1.361	1.703	2.053	2.98
	0.1	0.002	0.275	0.592	0.812	1.069	1.334	1.375	1.526
	0.05	0.02	0.204	0.317	0.465	0.512	0.597	0.680	0.730
	0.0	0	0	0	0	0	0	0	0

Supplementary Table 2. O.D₆₀₀ (A.U.) for Fig. 1i.

		Triplicates of O.D measurement				
		#1	#2	#3	Ave	SD
Galectin-3 (μM)	5	0.013	0.010	0.007	0.010	0.003
	10	0.128	0.268	0.192	0.196	0.070
	20	1.092	0.835	0.980	0.969	0.129
	40	2.927	2.978	3.046	2.984	0.060

Supplementary Table 3. O.D₆₀₀ for Fig. 5a.

		Triplicates of O.D measurement				
		#1	#2	#3	Ave	SD
Construct (40 μM)	wt-FL	2.905	3.086	3.034	3.008	0.093
	NTD	0.029	0.061	0.023	0.038	0.020
	CRD	0.039	0.003	0.023	0.022	0.018
	W/G-FL	2.172	1.938	1.841	1.984	0.170
	Y/G-FL	0.008	0.004	0.014	0.009	0.005
	WY/G-FL	0.005	0.003	0.006	0.008	0.002

Supplementary Table 4. UniProt entries for the sequences shown in Fig. 3a

Species	Entry	Entry name
<i>Homo sapiens</i> (Human)	P17931	LEG3_HUMAN
<i>Oryctolagus cuniculus</i> (Rabbit)	P47845	LEG3_RABIT
<i>Rattus norvegicus</i> (Rat)	P08699	LEG3_RAT
<i>Canis lupus familiaris</i> (Dog)	P38486	LEG3_CANLF
<i>Sus scrofa</i> (Pig)	A3EX84	A3EX84_PIG
<i>Bos taurus</i> (Bovine)	A6QLZ0	A6QLZ0_BOVIN
<i>Gallus gallus</i> (Chicken)	A4GTP0	A4GTP0_CHICK
<i>Xenopus laevis</i> (frog)	Q7ZSY1	Q7ZSY1_XENLA
<i>Danio rerio</i> (Zebrafish)	F1QSL3	F1QSL3_DANRE

Supplementary Table 5. Primers used in this study

Construct	Template	Primer Sequence
NTD-WY/G	pHD-Gal3-WY/G	Fw: 5' CTGGGTAACTCGAGCACCAC 3' Rv: 5' AGTTACCCAGCAGGGGGC 3'
NTD-Y/G	pHD-Gal3-NTD-Y/G	Fw: 5' CCTGGCGCATGGGGAAACCAGCCTGCT 3' Rv: 5' TGCGCCAGGCCATCCTTGAGGGTTGG 3'
NTD-W/G	pHD-Gal3-NTD-W/G	Fw: 5' CCTGGCGCAGGCGGGAAACCAGCCTGCT 3' Rv: 5' TGCGCCAGGGCCTCCTTGAGGGTTGG 3'
NTD-GFP	pHD-Gal3-NTD-GFP	Fw: 5' CTAGGTACCATGGATCAAAGGAGAAGAG 3' Rv: 5' CTAGGTACCCCCAGCAGGGCGCCATA 3'
Y/G	pHD-Gal3-WY/G	Fw: 5' CCTGGCGCATGGGGAAACCAGCCTGCT 3' Rv: 5' TGCGCCAGGCCATCCTTGAGGGTTGG 3'
W/G	pHD-Gal3-wt	Fw: 5' CCTGGCGCAGGCGGGAAACCAGCCTGCT 3' Rv: 5' TGCGCCAGGGCCTCCTTGAGGGTTGG 3'

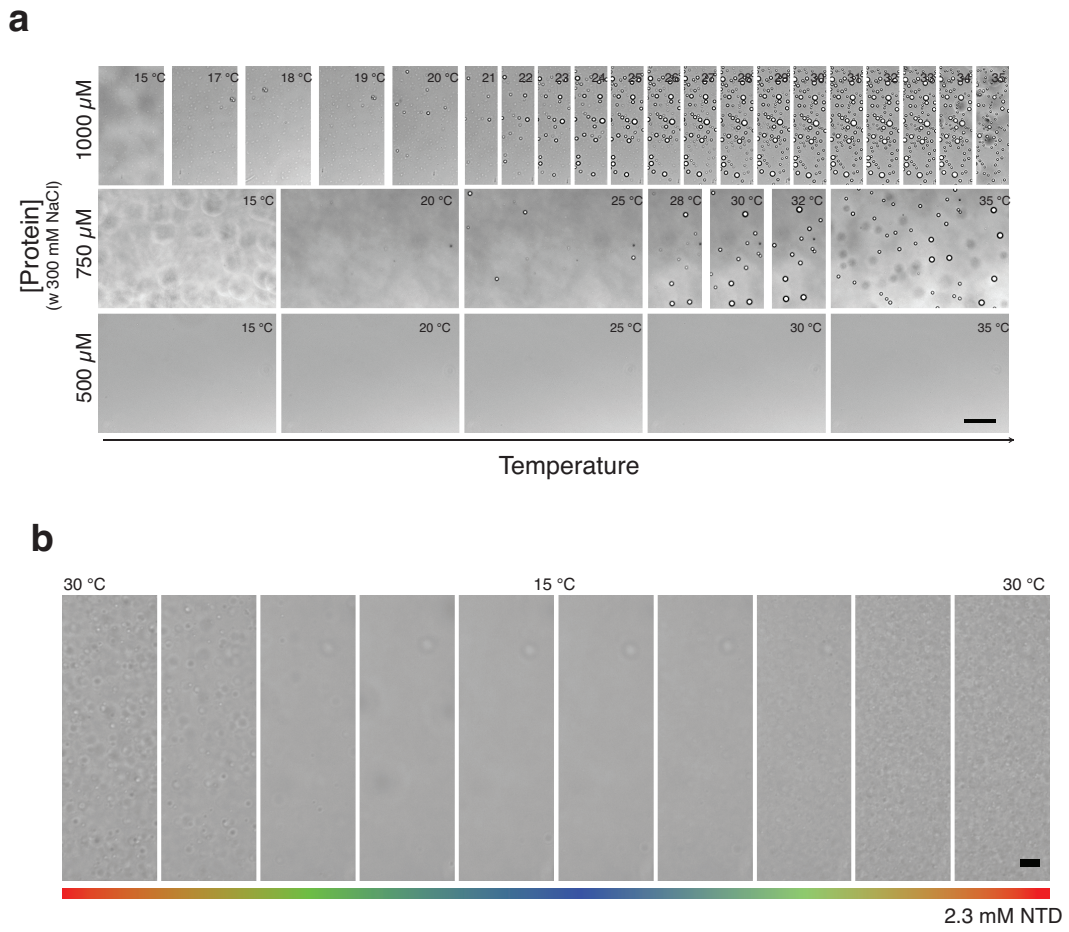
Supplementary Note 1. Estimate of the local galectin-3 concentration on the surface of the micelles

The radius of gyration of galectin-3 CRD is about 15 Å. The maximum distance between a pair of atoms in the CRD is around 35 Å. Two galectin-3 molecules bind either on the same LPS molecule or adjacent LPS molecules on a micelle, 50 Å × 50 Å × 100 Å is an overestimate of the space taken up by two CRDs in close proximity. A rough estimate of the local concentration is therefore:

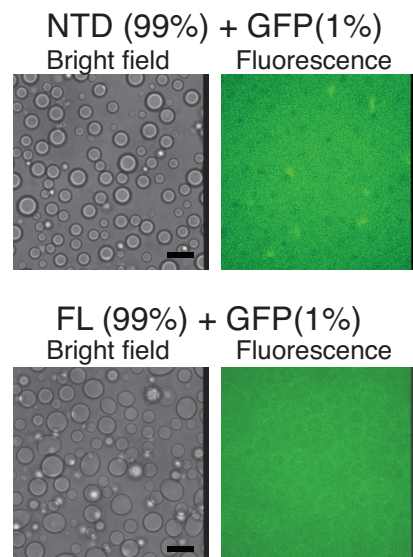
$$\frac{\frac{2}{6 \times 10^{23}} \text{(mole)}}{50(\text{\AA}) \times 50(\text{\AA}) \times 100(\text{\AA}) \times 10^{-27} \left(\frac{\text{L}}{\text{\AA}^3}\right)} = \frac{1}{75} \text{(M)} \approx 13.3 \text{(mM)}$$

Supplementary Note 2. The synthesized cDNA of the WY/G construct.

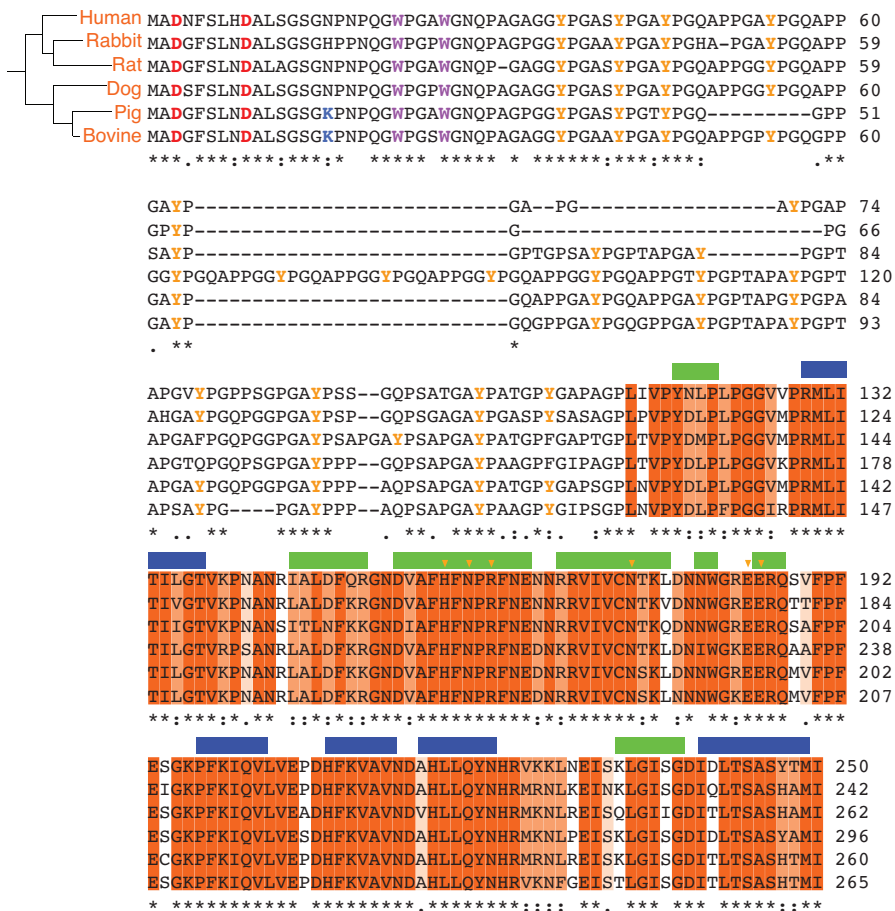
ATGGCAGACAATTTCGCTCCATGATGCGTTATCTGGGTCTGGAAACCCAAACCCCT
CAAGGAGGCCCTGGCCAGGCAGGAACCAGCCTGCTGGGGCAGGGGGCGGCCAGGG
GCTTCCGGCCCTGGGCCGGCCCCGGCAGGCACCCCCAGGGCTGGCCCTGGACAG
GCACCTCCAGGCCGGCCCTGGAGCACCTGGAGCTGGCCCCGGAGCACCTGCACCT
GGAGTCGGCCCAGGGCCACCCAGCGGCCCTGGGGCCGGCCATCTCTGGACAGCCA
AGTGCCACCGGAGCCGGCCCTGCCACTGGCCCCGGCGCCCTGCTGGGCCACTG
ATTGTGCCTTATAACCTGCCTTGCCTGGGGAGTGGTGCCTCGCATGCTGATAACA
ATTCTGGGCACGGTGAAGCCAATGCAAACAGAATTGCTTAGATTCAAAGAGGG
AATGATGTTGCCTTCCACTTTAACCCACGCTTCAATGAGAACACAGGAGAGTCATT
GTTTGCAATACAAAGCTGGATAATAACTGGGAAGGGAAAGAAAGACAGTCGGTTTTC
CCATTGAAAGTGGAAACCATTCAAATACAAGTACTGGTTAACCTGACCACTTC
AAGGTTGCAGTGAATGATGCTACTTGTGCAGTACAATCATGGGTTAAAAAACTC
AATGAAATCAGCAAATGGGAATTCTGGTGACATAGACCTCACCAGTGCTTCATAT
ACCATGATATAA



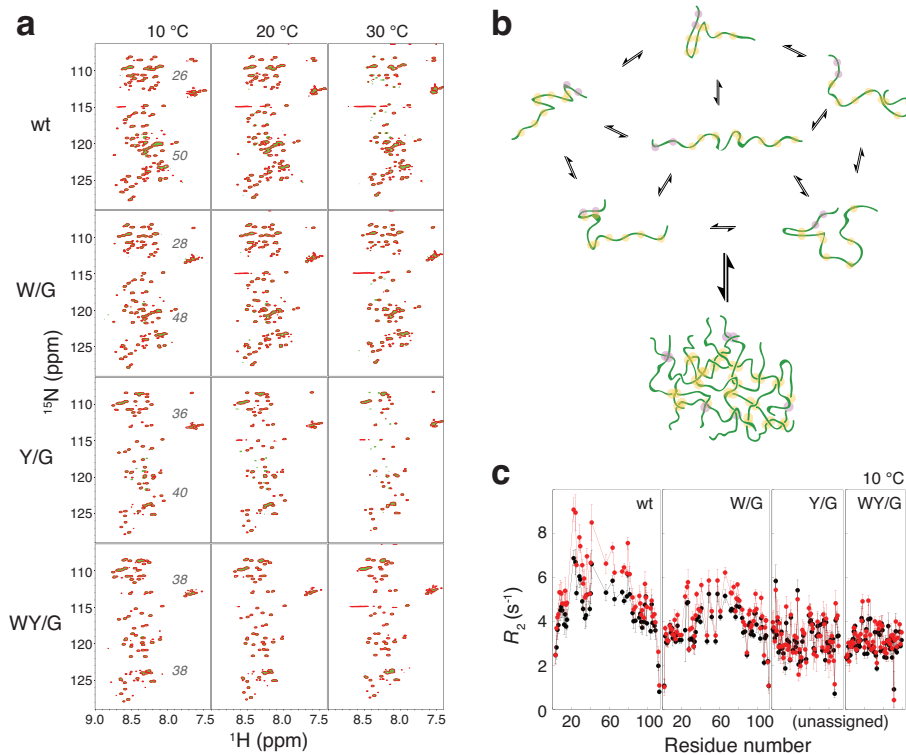
Supplementary Figure 1. (a) The effects on condensate formation of protein concentration and temperature (at a fixed salt concentration of 300 mM). Scale bar: 50 μ m. (b) The LLPS of 2.3 mM NTD in the absence of NaCl. Scale bar: 10 μ m. Experiments were performed at least three times for each protein sample.



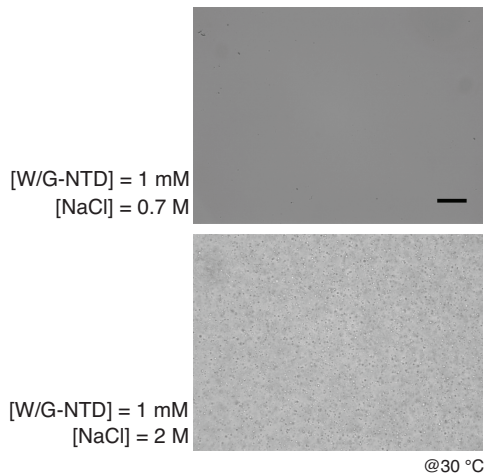
Supplementary Figure 2. The NTD and full-length samples under the conditions of the two-phase regime mixed with 1 % of GFP. GFP has no preference to enter the condensate in both instances (see Fig. 2c, 2h of GFP-tagged NTD for comparison). Scale bar: 50 μ m. These control experiments were performed once.



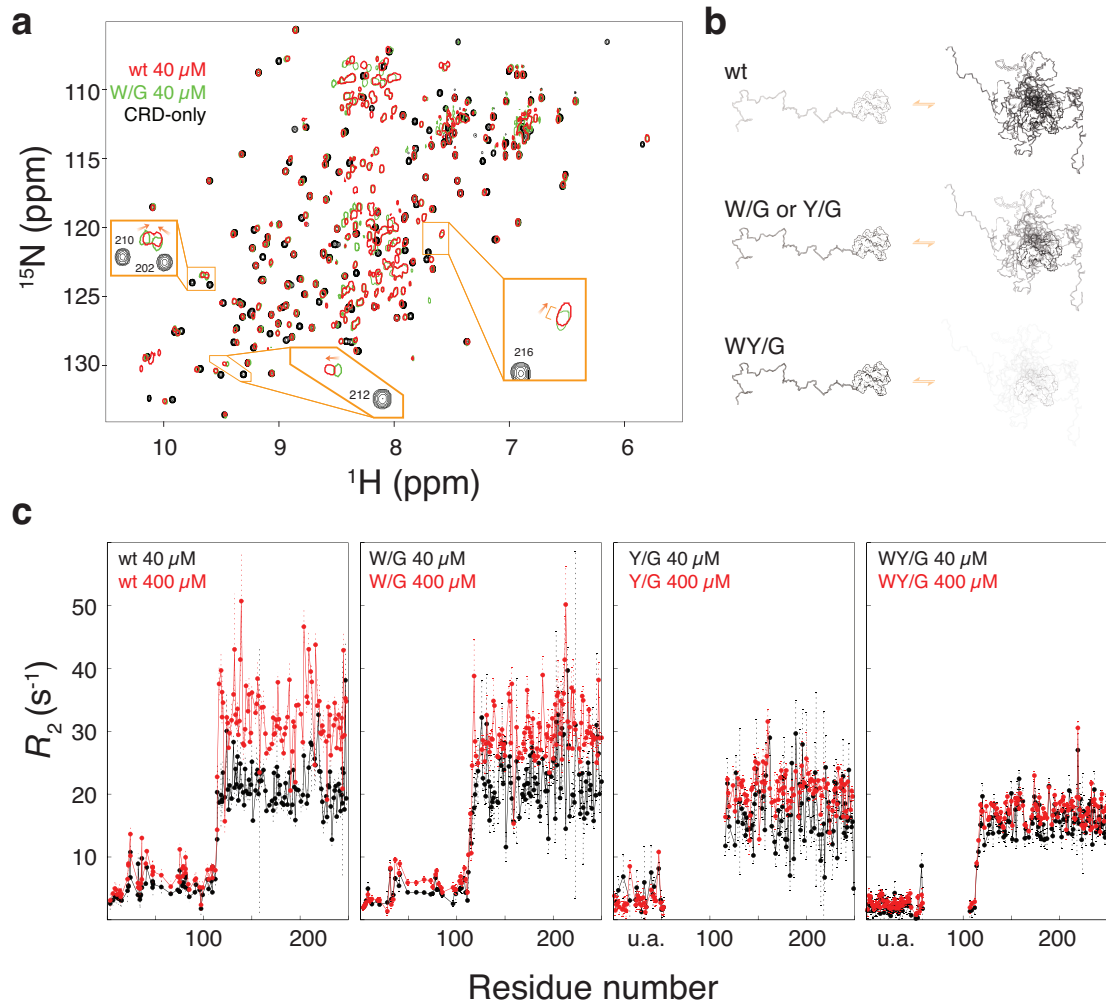
Supplementary Figure 3. Comparison of representative mammalian galectin-3 amino-acid sequences. The residues in the carbohydrate-recognition domain are highlighted with dark, medium, or light orange depending on the level of conservation. Negatively charged, positively charged, tryptophan, and tyrosine residues in the N-terminal domain are shown in red, blue, purple and yellow, respectively.



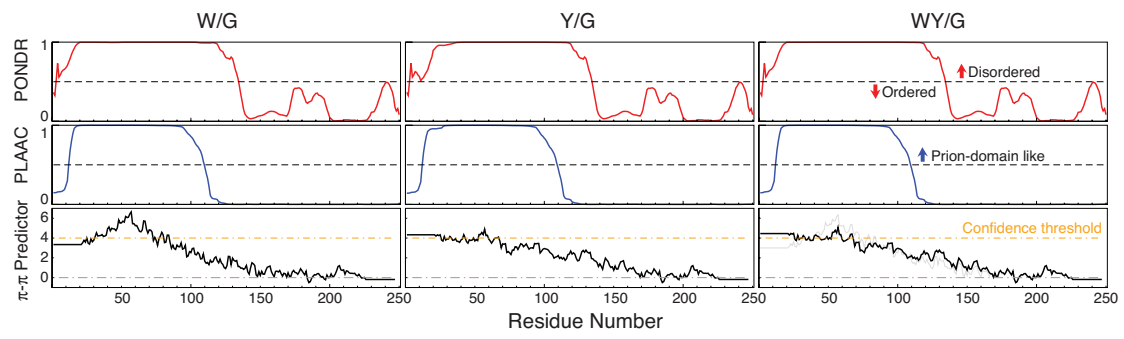
Supplementary Figure 4. NMR studies of N-terminal domain (NTD) constructs of galectin-3. (a) HSQC spectra of 40 (green) or 400 μ M (red) samples of the different constructs at different temperatures. The expected numbers of peaks from glycine (upper number) and other residues (lower number) are shown in the spectrum recorded at 10°C for each construct. There are more peaks than expected for the wild type because the conformation changes at equilibrium occur in the slow exchange regime (vs the NMR timescale). This exchange probably involves the aromatic residues because when they are all removed, most of the extra peaks disappear (WY/G spectra). (b) Schematic representation of inter- and intramolecular NTD interactions through aromatic residues. (c) Transverse relaxation rate constants (R_2) of 40 μ M (black) and 400 μ M (red) samples of the different constructs at 10°C. The overall reduction in R_2 vs the wild type for the constructs without aromatic residues indicates that inter- and intramolecular conformational exchanges are abolished.



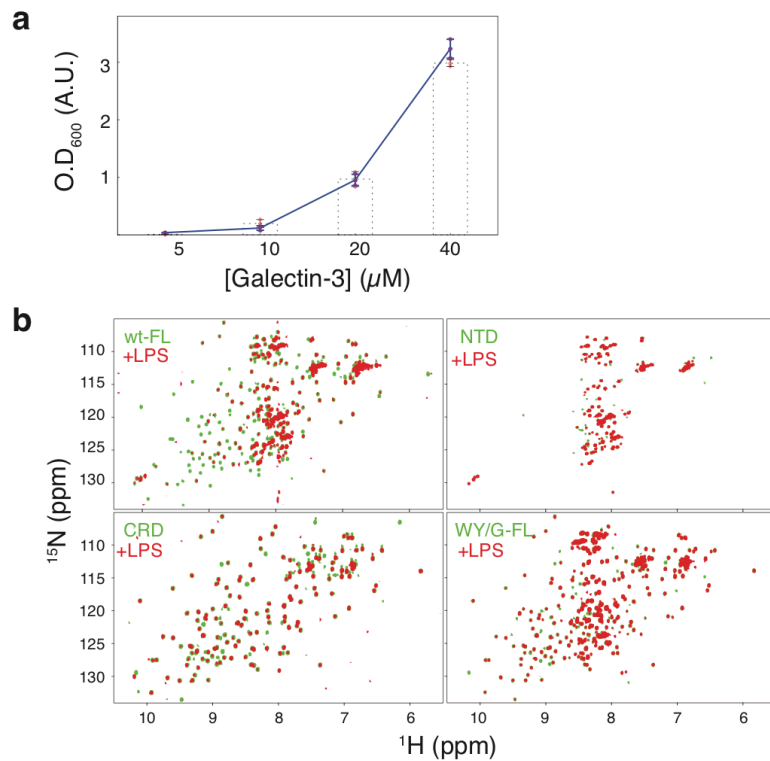
Supplementary Figure 5. The micrographs of 1 mM W/G-NTD construct. The 1 mM wild-type sample phase-separated when the NaCl concentration is above 0.15 M, but even with 0.7 M salt, W/G-NTD remains in the one-phase regime. When the NaCl concentration is 2 M, the W/G-NTD construct shows condensate probably due to the contribution of tyrosines because there is no condensate for the WY/G-NTD construct under the same condition (Fig. 3e). Scale bar: 50 μ m. Experiments were performed at least three times for each protein sample.



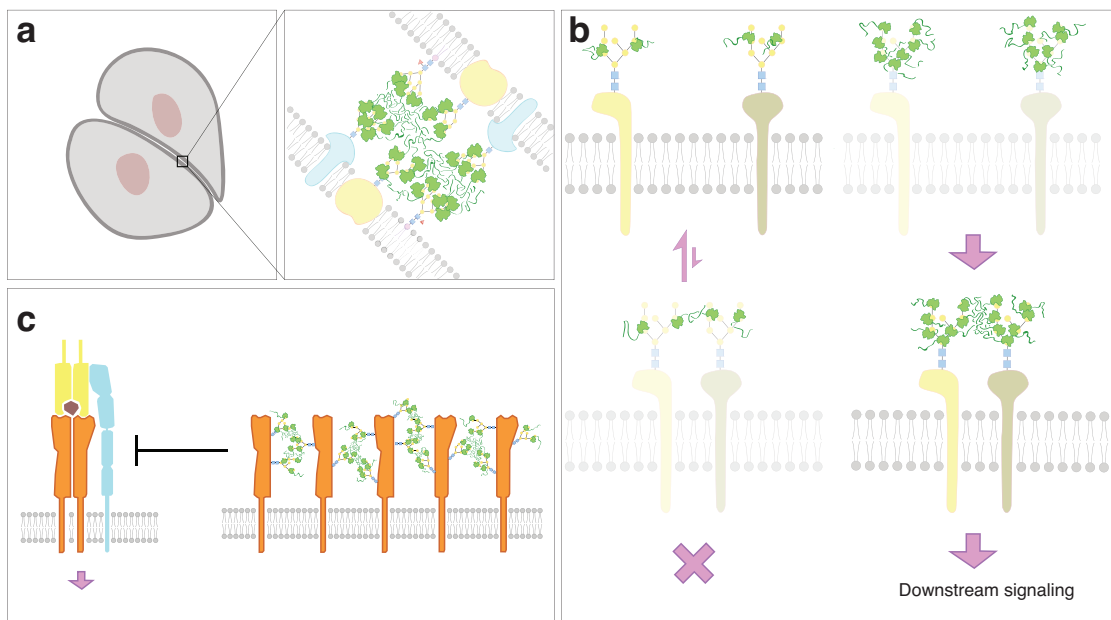
Supplementary Figure 6. NMR studies of full-length galectin-3 constructs. (a) Comparison of HSQC spectra of 40 μM samples of the wild type (red) and of the W/G (green) construct with that of a carbohydrate recognition domain (CRD)-only construct. The changes in chemical shift (orange arrows) indicate more N-terminal domain (NTD)-CRD interactions in the wild type than in the W/G mutant. These interactions are abolished in the WY/G construct (see the main text). (b) Illustration of the proposed equilibrium population distributions of the wild type and the two constructs between the fully extended conformation and one with NTD-CRD interactions. The darker image represents the higher population. (c) Transverse relaxation rate constants (R_2) for wild type galectin and the three constructs at 40 μM (black) and 400 μM (red). As in Fig. S4c, the overall R_2 decreases when the aromatic residues are replaced with glycine. These results reinforce the conclusion that protein dynamics increase as inter- and intramolecular interactions become rarer.



Supplementary Figure 7. Sequence analyses of aromatic-substituted mutants of the level of structural disorder, similarity to prion-like proteins, and the propensity to form π - π interactions



Supplementary Figure 8. (a) Turbidity (O.D_{600nm}) measured under different galectin-3 concentration in the presence of 300 mM NaCl (blue lines, n=3 independent samples; data are presented as mean values +/- SD) in comparison to without NaCl (dashed black bars, also see Fig. 1i). (b) NMR studies of lipopolysaccharide (LPS)/galectin-3 mixtures. HSQC spectra of 40 μM samples in the absence (green) or in the presence of LPS micelles (red).



Supplementary Figure 9. Schematic illustrations of how multiple weak interactions can collectively mediate galectin-3 functions: (a) cell-cell adhesion, (b) signal activation, and (c) signal inhibition.